RSC Advances

ROYAL SOCIETY OF CHEMISTRY

www.rsc.org/advances

The optical properties of low infrared transmittance WO_{3-x} nanocrystal thin films prepared by DC magnetron sputtering under different oxygen ratios

Yunchuan Xin[a,b], Huaijuan Zhou[a,b], Xiaojie Ni[c,d], Ying Pan[a], Xiaoli Zhang[a,b], JianYun Zheng[a,b], ,Shanhu Bao[a,*] Ping Jin[a]

[a] State Key Laboratory of High Performance Ceramics and Superfine Microstructure, Shanghai Institute of Ceramics, Chinese Academy of Sciences, Shanghai 200050, China

[b] Graduate School of Chinese Academy of Sciences, Beijing 100049, China

[c] State Key Laboratory of Particle Detection and Electronics (IHEP&USTC), University of Science and Technology of China, Hefei 230026, China

[d] Department of Modern Physics, University of Science and Technology of China, Hefei 230026, China

[*] Corresponding Author at: State Key Laboratory of High Performance Ceramics and Superfine Microstructure, Shanghai Institute of Ceramics, Chinese Academy of Sciences, Shanghai 200050, China. Tel.: +86 21 69906206. Fax: +86 21 69906221.

E-mail: shanhu.bao@mail.sic.ac.cn

Abstract

The low infrared transmittance WO_{3-x} (0<x<1) nanocrystal thin films were prepared by DC magnetron sputtering under different Ar-O_2 ratios, as transparent conductors with high transmittance in visible range and UV blocking. The infrared shielding properties could be adjusted by tuning the oxygen ratio during sputtering process. The intrinsic defects, such as oxygen vacancy ($V_o^{\cdot\cdot}$) and special atom (W^{5+}), determine the main optical properties by localized states originated from the electron caused by interband transition and the surface dipole of the plasmon oscillation of the nanoparticle with optical scattering. The structures, morphology, defects and chemical states were investigated. With respect to oxygen ratio, it has little effect on the structure and morphology, yet the optical shielding performance, defects and chemical states can be controlled linearly just considering the oxygen ratio during sputtering process. The WO_{3-x} thin films have great potential for the applications in infrared shielding and energy conservation.

Introduction

The issues of solar energy utilization and energy savings have attracted the worldwide attention. Transparent conductors (TCs) have a multitude of applications for these [1]. The largest of these applications make use of the fact that the TCs have low infrared emittance and hence can be used to improve the thermal properties of modern fenestration. The TCs films include sliver-based films [2, 3], SnO-based (ITO, FTO) films [4-6], ZnO-based (AZO) films [3, 7] VO_2-based films[8] and WO_3-based films[9]. Tungsten oxide, however, has obtained widespread applications in electrochromic materials [1, 9-13], smart windows [14], gas sensors [15, 16], photo catalyst [17, 18], thermal control of satellites [19], infrared camouflages [20], and shielding [21].

The optical shielding properties of WO_{3-x} can be regulated by the electron concentration. In the case of x=0 [14], it is these electrons that trigger the color change by occupying localized states and absorbing near-infrared (NIR) light of ~1.4 eV through a small polaron mechanism mainly in an amorphous WO_3, or by resonating in the conduction band as free electrons and absorbing NIR light of ~0.7 eV mainly in a crystallized WO_3 [11, 22]. This theory also can be applied to WO_{3-x} and intercalated MWO_3 (M: H, Li, Na, K, Cs, Ti, Ta, etc.) materials. The traditional doping method changes the electron concentration by introducing extra electrons. A better and more straightforward approach is to produce intrinsic defects by forming WO_{3-x} directly. However, the former researches have almost focused on the doping MWO_3 materials [22-26], yet it is rare about infrared-shielding WO_{3-x} without doping, especially for the WO_{3-x} thin films prepared by the magnetron sputtering approach (suitable for

mass production), which makes the optical properties easily tuned just by adjusting intrinsic defects of the films through controlling the sputtering process. Moreover, the WO_{3-x} thin film is directly obtained by reactive magnetron sputtering at room temperature. This process is easy controllable.

In our experiment, the sub-stoichiometry tungsten oxide (WO_{3-x}) thin films, which exhibited low infrared transmittance, were prepared by tuning the Ar-O_2 ratio during sputtering process. The thin films had similar optical properties on the infrared shielding as the reported $CsWO_3$ [22], as well as high transmittance in visible range and UV blocking. The structures and morphology were determined. The relationships between defects (oxygen vacancy and special tungsten atom) and oxygen ratio were investigated with variable energy positron annihilation spectroscopy and X-ray photoelectron spectroscopy. The low-infrared-shielding properties could be served for solar energy utilization and energy savings, such as buildings, automobile, satellite technology etc.

Experiment

Preparation of WO_{3-x} films

The tungsten oxide thin films were prepared by reactive DC magnetron sputtering under different oxygen ratios on quartz and Si (100) substrates at room temperature. The background pressure of sputtering cavity was maintained at 1×10^{-5} Pa for 72 hours to purify the cavity in prior to deposition. The tungsten (>99.9%) targets was employed. The power of tungsten was kept at 100 W and the pressure was maintained at 0.6 Pa during sputtering. The ratios of Ar:O_2 changed from 60 : 3

sccm to 60 : 6 sccm, then the films were annealed at 750 K under 500 Pa for 5 minutes. For simplification, the samples with the Ar:O_2 ratios of 60 : 3 sccm, 60 : 4 sccm, 60 : 5 sccm and 60 : 6 sccm annealed at 500 Pa were labeled as S1, S2, S3 and S4, respectively. The sample with the Ar:O_2 ratio of 60 : 3 sccm annealed in air was labeled as S1-air. All the samples` thickness were controlled at ~200 nm.

Characterization of samples

The transmittance and the reflectance spectrum were investigated by the UV4100 (HITACHI) spectrograph from 350 nm to 2600 nm. The sheet resistance was tested by four probe method. The ellipsometer (J.A. Woolam Co. Inc. M2000 ellipsometer) was employed to investigate the optical constant: the refractive index, n and extinction coefficient, k with incidence angles of 60º and 70º to the films at room temperature in the wavelength ranges from 240 nm to 1680 nm (0.7 eV < ω < 5.1 eV). The ellipsometric data (Ψ, Δ) was recorded at each data point for the most critical data. The microstructure were studied by X-ray diffraction (XRD, a Rigaku Ultima IV diffractometer with grazing angle mode using Cu *K*α radiation, λ = 0.15418 nm). The morphology was characterized by scanning electron microscope (SEM, HITACHI SU8220). The film defects were investigated by using variable energy positron annihilation spectroscopy (VEPAS). The X-ray photoelectron spectroscopy (XPS, Thermo Fisher Scientific Co. Inc. ESCAlab250) was employed to study the chemical states and electronic structures.

Results and discussion

The stoichiometric tungsten trioxide film is yellowy. It possesses a band gap of

2.62 eV and is transparent in a wide range from green to near-infrared light [27]. It was also verified in our experiment (refer to the transmittance curve of the sample S1-air. (**Fig. 1 (b) the cyan line**)). Yet the sub-stoichiometric tungsten oxide thin films revealed opposite optical properties. The samples (S1~S4) deposited in different oxygen partial pressures presented serial optical properties of various degree reflection and transmission. The transmittance of the samples, whose oxygen ratios were below 3 sccm, were under 20% in the visible range. (Their transmittance spectrum were attached in the supplementary information). As the oxygen flow increased from 2 sccm to 3 sccm, a huge increase happened in the visible range. As the **Fig. 1 (a)** and **(b)** described, the transmittance spectrums extended shielding to near-infrared range of solar spectrum. The transmittance curves demonstrated downward interference peaks, due to the existence of interference from 480 nm to 550 nm, but it did not affect the performance. High transmittance in visible range and low transmittance in near infrared range were demonstrated. The difference between visible and near-infrared ranges was used in infrared shielding [28-30], such as the energy conservation in buildings. In summer, the sunlight flows into the house, but the heating parts of solar spectrum will be isolated out of door. Nevertheless the long wavelength heating infrared will be retained at room in winter. This is very beneficial for energy conservation without significant influence on lighting. The infrared blocking was achieved by reducing the oxygen ratio. The reflectance also rose, accompanied the descendent ratios. The transmittance of S1 in the visible light region was ~ 60% (550 nm, excluding the influence of interference), and 8%~22% in

the near infrared (800 nm to 2600 nm) region. The reflectance of this sample was 15%~41% from the wavelengths of 800 nm to 2600 nm. At the same time, all the samples` transmittance depicted strong downtrend below 400 nm, which indicated that the thin films cut off the ultraviolet radiation.

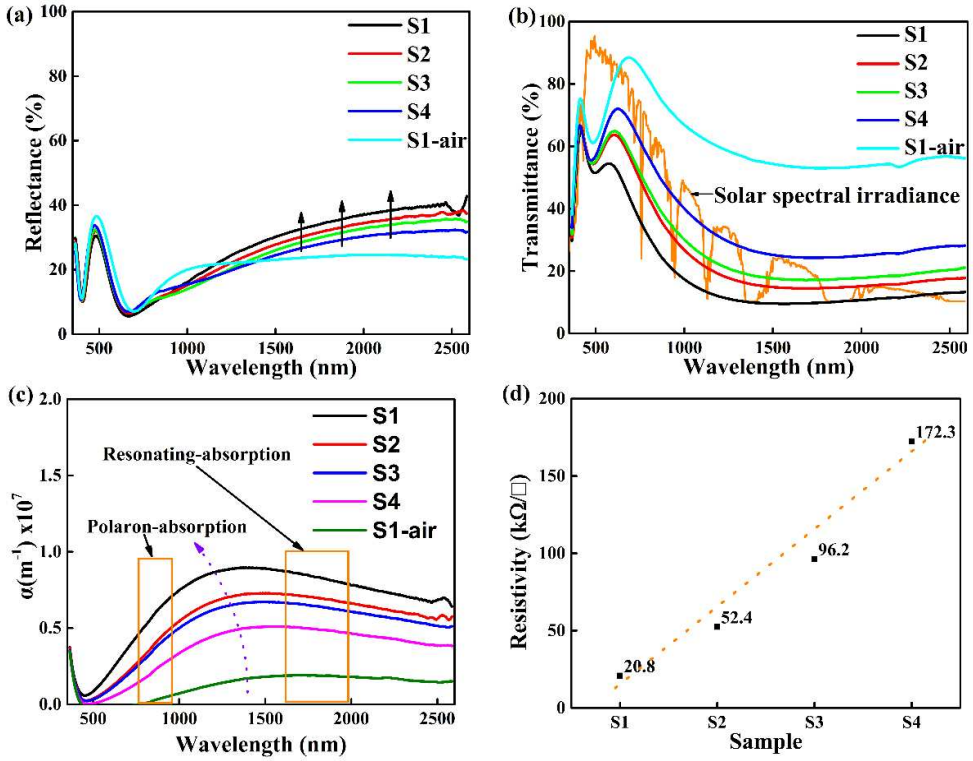

Fig. 1: The reflectance (a), transmittance (b), absorbance (c) and square slice resistance (d) of prepared samples sputtered under different oxygen ratios.

The absorption coefficient, α [14] as a function of wavelength λ is computed by

$$\alpha(\lambda) = \frac{1}{d}\ln\left(\frac{1-R(\lambda)}{T(\lambda)}\right) \quad (1)$$

where d is the thickness of film. The thickness of film is measured by SEM. The optical absorption below E_g follows an exponential behavior[31]. For tungsten oxide, in the E_g region (high absorption) or above the fundamental absorption edge, the

absorption follows a power law of the form [32]

$$(\alpha\ h\upsilon) = B(h\upsilon - E_g)^2 \qquad (2)$$

where *hv* is the energy of the incident photon; *α* is the absorption coefficient; *B* is the absorption edge width parameter and E_g is the band gap. The optical absorption coefficient, *α*, has been given in **Equation (1)**. The E_g values, determined by extrapolating the linear region of the plot to *hv* = 0, decreased from 2.96 eV (419 nm) to 2.68 eV (463 nm) with the increment of oxygen partial pressure. The inverse correlation between oxygen content and E_g found in WO_{3-x} films suggested that the regulation of transmittance and reflectance were achieved by only adjusting the percentage of oxygen.

The mechanism of conducting and tuning optical properties originated from the electron caused by interband transition from semiconductor tungsten oxide. For sub-stoichimetric tungsten oxide, however, the defects, such as oxygen vacancy and special tungsten atoms, should be taken into consideration. It had been reported that localized states were located close to an oxygen vacancy or a special W atom[11]. An electron was transferred from one localized state to a neighboring one. For the stoichiometric tungsten oxide, the states were localized on the W sites [33]. In the case of the sub-stoichiometric WO_{3-x}, the oxygen vacancy states had the equivalent influence on the transitions. The localization of an electron from the conduction band was introduced by the strong electron-phonon interaction[34]. The absorbance happened in the polaron-absorption areas (**Fig. 1(c)**). However, it was also reported that the optical scattering of the tungsten oxide film in the near-infrared region

resulted from a surface dipole mode of the plasmon oscillation of the nanoparticle (or nanocrystal) by Yohei Sato etc. [23]. The carrier electron density of the tungsten oxide nanoparticle was the primary factor in the condition of the surface plasmon resonance. The scattering peak energy was usually designed in the energy range from the visible to near-infrared regions by controlling the carrier density. The absorbance, which derived from the surface plasmon oscillation of the nanoparticle, occurred in the resonating-absorption areas (**Fig. 1(c)**). In the sub-stoichiometric tungsten oxide film, the carrier density was controlled by the defects, primarily referring to the oxygen vacancy and special tungsten atoms. From the point of electric neutrality, the special tungsten atoms were related to oxygen vacancies. If the carrier electron density was suitable in the near-infrared region, the material would have more efficient scattering ability, with low transmittance in near-infrared resonance. As it was demonstrated in the **Fig. 1 (c)**, the scattering moved toward the visible range. While for the ultraviolet range, the energy of photon surpassed the absorption edge, the ultraviolet radiation was cut off.

Another characterization method about carrier electron density was electron resistivity. The square slice resistance of thin films were measured by four probe method. The result was denoted in **Fig. 1 (d)**. The resistances was in direct proportional to the oxygen ratios. The resistance of the sample annealed in air (S1-air) was too big to exceed the measuring range, which was not added. The sample of S1 delivered the smallest resistivity. The low oxygen ratio during sputtering process would lead to more defects, and smaller resistivity.

Ellipsometry measurements were carried out in a rotating analyzer variable-angle spectroscopic ellipsometer. This instrument measured the ratio of the complex Fresnel reflection coefficients *R* of parallel (*p*) and perpendicular (*s*) polarized light. This ratio defines the ellipsometric angles $\Psi(\omega)$ and $\Delta(\omega)$ according to

$$\frac{R_p}{R_s} = \tan[\Psi(\omega)]\exp[i\Delta(\omega)] \quad (3)$$

The dielectric function $\varepsilon(\omega) = \varepsilon_1 + i\varepsilon_2$ could be adequately parametrized with a Lorentz-Drude (LD) Mode:

$$\varepsilon(\omega) = \varepsilon_\infty - \sum_{i=1}^{N} \frac{\omega^2_{p,i}}{\omega^2 + i\omega/\tau_i} + \sum_{j=1}^{M} \frac{f_j}{\omega^2_j - \omega^2 - i\Gamma_j\omega} \quad (4)$$

where the constant ε_∞ accounts for excitations far above 5.1 eV; the N Drude terms describe the free-carrier response with $\omega_{p,i}$ the plasma frequency of the ith Drude term and τ_i the relaxation time; the M Lorentz terms represent the effect of interband transitions with f_j the intensity of the jth oscillator, ω_j its energy, and Γ_j its broadening. The relation between the dielectric function and the refractive index n and extinction coefficient k is $\varepsilon_1 = n_2 - k_2$ and $\varepsilon_2 = 2nk$. The value of *n*, *k* was fitting by the software ***CompleteEASE*** (J.A. Woollam Co. Inc.).

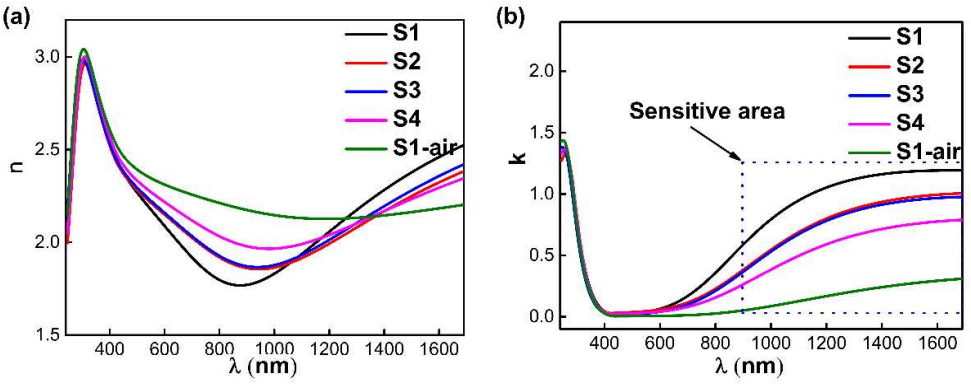

Fig. 2: The optical constant of tungsten bronze thin films with respect to the oxygen ratio by the ellipsometry.

The extinction coefficient (*k*) represented the interaction degree between wave and materials. As it was shown in **Fig. 2**, the oxygen ratios had little influence on the refractive index (*n*) and extinction coefficient (*k*) in the visiable range. While in the near-infrared range, they were poles apart. The sub-stoichiometric tungsten oxide had large extinction coefficient *k*. The electron-photon interactions were influenced by located states caused by intrinsic defects and small polarons from crystal, which was adjusted directly by oxygen ratio. The oxygen ratio affected the infrared shielding ability of thin films.

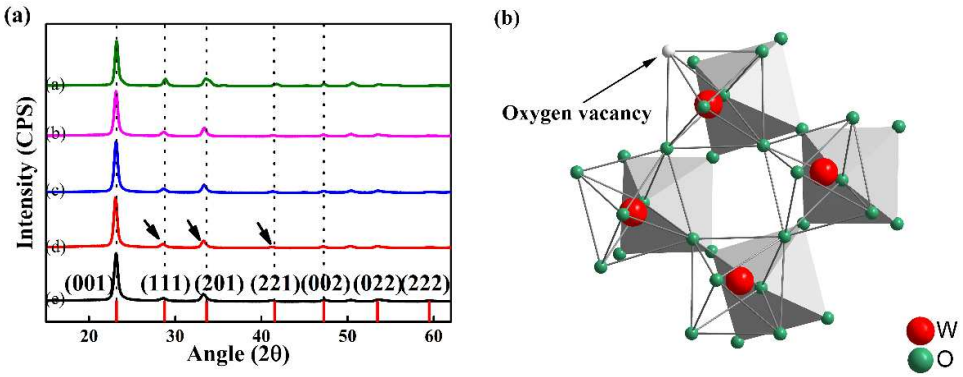

Fig. 3: (a) The X-ray diffraction patterns of WO_{3-x} films with 204 nm thickness on quartz substrate. (b) The spatial structure diagram of tungsten bronze.

The XRD patterns of the thin films deposited on quartzes were depicted in **Fig. 3(a)**, in order to reveal the relationship between optical properties and structure. The thin films annealed at 750 K formed orthorhombic phase (PDF #20-1324) in accord with Ref [35, 36]. Some peaks ((111), (201), (221) etc.) had drifted toward small angle

areas because of the existence of a small amount of amorphous phase in the crystal films and lattices relaxation. For the sub-stoichiometric tungsten oxide, the ingredients should be WO_{3-x} ($0<x<1$) (That had been proved by XPS in the article later), but the structure pattern was not consistent with that of WO_{3-x} (PDF #53-0434). All the samples had the same lattice structure no dependence of the oxygen ratio. In other words, the oxygen contents had no remarkable influences on the thin film lattice. The structure of tungsten bronze (WO_6) was octahedral, which was exhibited in **Fig. 3(b)**. The interval of WO_6 and interspace between WO_6 provided the tunnels for ion transportation and occupation. It was to the benefit for the intrinsic defects.

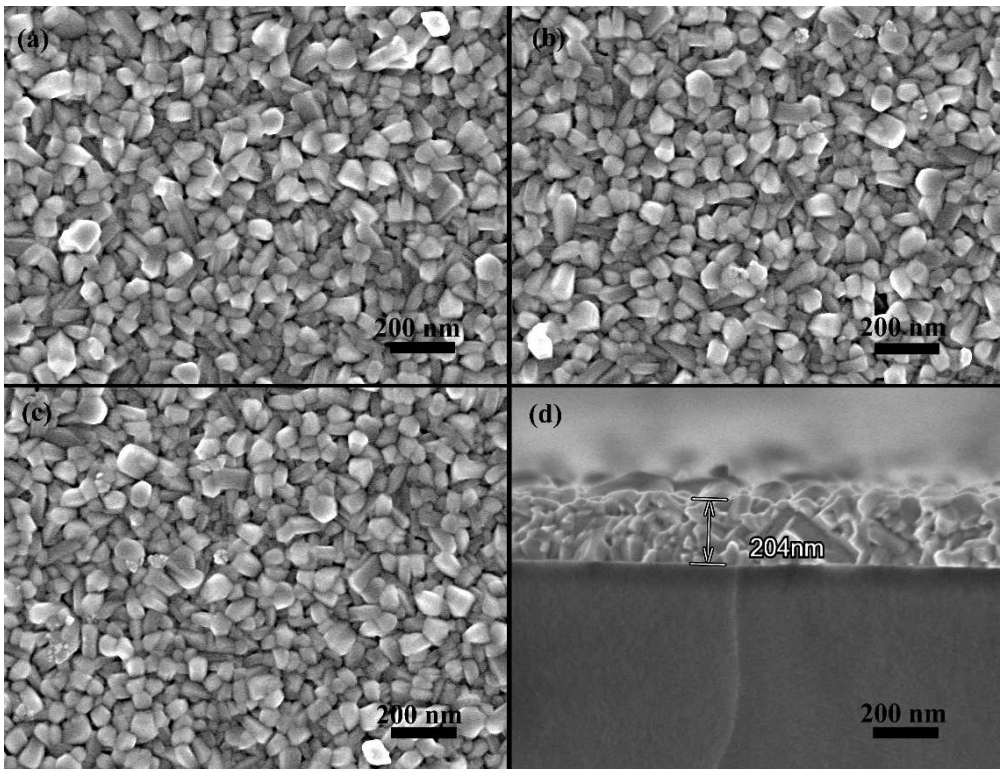

Fig. 4: The surface morphology of the samples S1 (a), S4 (b) and S1-air (c); the cross-section photograph of S1 (d). (The morphology before annealing was attached in the supplementary information)

After the thermal treatment under 500 pa, all the samples were still parallel of their morphology. The sample S1-air, that was heat in air, was also in agreement with others. Therefore, the surface photographs only from three samples (the ratio: 60:3, S1; 60:6, S4; 60:3-air, S1-air) were exhibited at **Fig. 4(a), (b)** and **(c)** respectively. **Fig. 4(d)** was the cross-section photograph of sample S1. The change of oxygen ratio could not affect the lattice parameters and morphology of tungsten bronze, which verified the results of XRD. The crystal boundary was not very distinct as there were parts of amorphous phase attached. The amorphous tungsten bronze acted an important role in optical process. It was these amorphous particles that offered the color change by occupying localized states and absorbed near-infrared (NIR) light of ~1.4 eV through a small polaron mechanism[22]. The amorphous nanoparticles had the same effects corresponding to the doping ions in MWO_3. For the crystallized WO_3, the interaction by resonating in the conduction band as free electrons absorbed NIR light of ~0.7 eV [22]. The thermal treatment at 750 K brought about parts of the particles crystallized. It was a nearly equals split between the amorphous WO_3 and crystallized WO_3. The electrons induced by defects through tuning oxygen ratio trigger the color change. The lower oxygen ratio led to more defects and therefore triggered more electrons transfer between the energy bands.

The chemical states of samples with different oxygen ratios were determined by XPS. In the XPS study, Ar^+ bombardment was used to peel away surface atoms. Since long-time Ar^+ bombardment changed chemical states[37], the surface processing time was under 5 s. The spectra were fitted on the basis of the parameters in **Table 1**. The

result was shown in **Fig. 5 (a)**, **(b)** and **(c)**.

Table 1

Overview of the W4f peak fit parameters for different oxygen ratios [37, 38].

Tungsten oxidation States	$W4f_{7/2}$ BE (eV)	%L-G	FWHM (eV)	$\Delta BE(W4f_{7/2}-W4f_{5/2})$ (eV)
W^{6+}	35.7±0.1	20	1	2.1±0.1
W^{5+}	34.6±0.2	20	0.7	2.1±0.1

Compared with sample S1, the area and the height of core level W^{5+} were decreased in S4, which implied the reduced defects. The evolution process of W oxidation states change was step by step related to the surroundings. The modulation of W^{5+}/W^{6+} could be associated with the oxygen ratio during the sputtering process. The samples annealed in air had little parts of W^{5+}, which indicated that the point defects, such as $V_o^{\cdot\cdot}$, $W_W^{'}$ almost disappeared. These W^{5+} could derive from the surface lattice distortion, open chemical bonds and Ar^+ bombardment, so the x value was not computed for accuracy. The W^{5+} atoms exist in the meantime of $V_o^{\cdot\cdot}$. A new band was brought in matching the polaron absorption, leading to low transmittance in infrared range.

Variable energy positron annihilation spectroscopy (VEPAS) [39-41] was employed for the first time to investigate the relationship between defects and oxygen ratio of the tungsten bronze. S is a parameter during VEPAS measurement. It is about the defects and phase-transformation, the formula form is

$$S = \frac{\int_{-a}^{a} C(E)\,dE}{\int_{-\infty}^{\infty} C(E)\,dE} \quad (5)$$

where C(E) is the experiment spectrum.

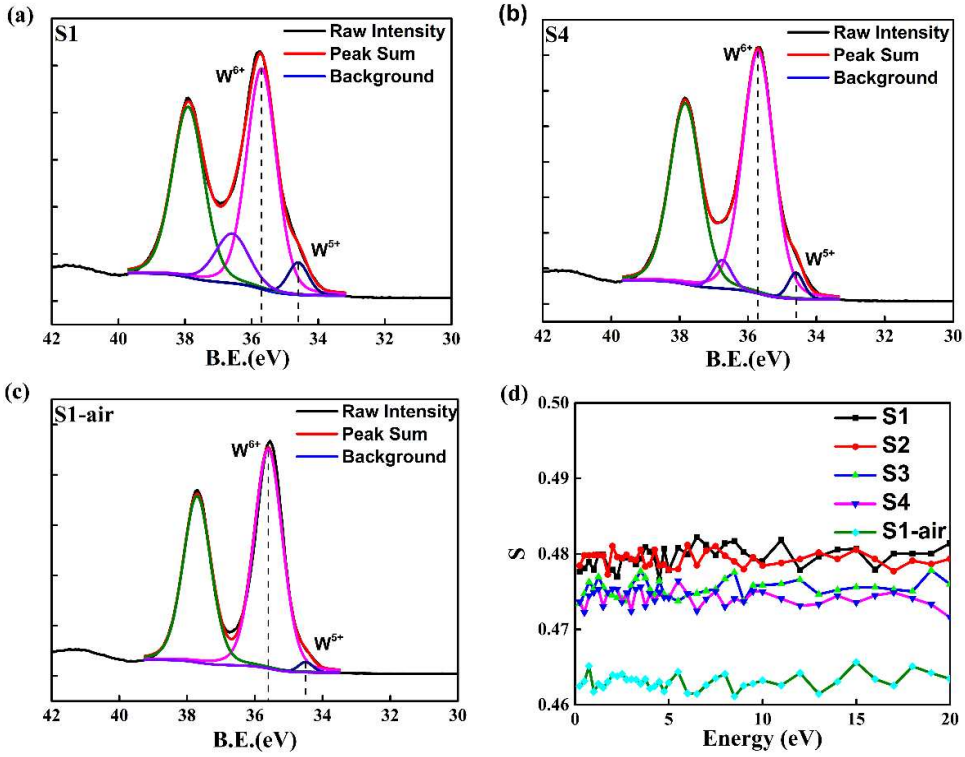

Fig. 5: Representative fitted W4f core level spectra of sample S1 **(a)**, S4 **(b),** S1-air **(c),** and S parameter vs energy **(d)**.

S parameter was directly proportional to the defects at the same condition of phase structures. However S parameter was not sensitive to anion defects. The thin films should be neutrality. The **equations (6) ~ (7)** below were very possible. If the localization states were considered, the **equations (8) ~ (9)** were also needed. The W^{4+}, W^{5+}, W^{6+}, $V_o^{\cdot\cdot}$, $V_o^{\cdot}$ existed in the tungsten bronze. For simplification, the **equations (8)** and **(9)** were ignored. To move forward a single step, the W^{4+} was also

taken out from the results of XPS. A conclusion could be obtained that cation defects, e.g. W^{+5}, were connected with the $V_o^{\cdot\cdot}$.

$$WO_3 \rightarrow WO_{3-x} + 2xW_W^{'} + xV_O^{\bullet\bullet} + \frac{x}{2}O_2 \uparrow \quad W:+5 \tag{6}$$

$$WO_3 \rightarrow WO_{3-x} + xW_W^{''} + xV_O^{\bullet\bullet} + \frac{x}{2}O_2 \uparrow \quad W:+4 \tag{7}$$

$$WO_3 \rightarrow WO_{3-x} + 2xW_W^{'} + yV_O^{\bullet\bullet} + (2x-y)V_O^{\bullet} + \frac{x}{2}O_2 \uparrow \quad W:+5 \tag{8}$$

$$WO_3 \rightarrow WO_{3-x} + xW_W^{''} + yV_O^{\bullet\bullet} + (2x-y)V_O^{\bullet} + \frac{x}{2}O_2 \uparrow \quad W:+4 \tag{9}$$

As it was depicted in **Fig. 5 (d)**, S parameter decreased with the increment of oxygen ratio, the defect amount of S1-air was minimum. The thin film with the ratio 60:3 had the largest S parameter averagely, which indicated the most defects exist in the film and therefore delivery the highest electron concentrations. It was these electrons that trigger the color change by occupying localized states and absorbing near-infrared (NIR) light of ~1.4 eV through a small polaron mechanism in WO_{3-x}, or by resonating in the conduction band as free electrons and absorbing NIR light of ~ 0.7 eV in a crystallized WO_3. The tiny change of oxygen ratio altered the optical properties of the thin films, which was similar to the doping treatment for semiconductor. In the **Fig. 3 (b)**, the defect sites were shown, W^{5+}, W^{6+} exist in the tungsten bronze on amount of electric neutrality. The special tungsten atoms were not shown, which leaped from one site to the neighbor one. It was not bound with the oxygen vacancy. Anyhow, there were more oxygen vacancies in the sample deposited at low oxygen ratio by sputtering.

Conclusions

In this work, low infrared transmittance thin films were prepared. The films had high transmission in visible range and cut off the ultraviolet radiation. The surface structure, optical properties and defects of the thin films were investigated. The amorphous nanoparticles of tungsten oxide sputtered by reactive DC magnetron sputtering transformed to nanocrystals after annealing. The oxygen ratio had much influences on the optical properties, but little influence on the lattice of tungsten bronze. Ellipsometry measurements indicated the thin films had almost the equivalent optical constant in the visible range, but the extinction coefficient of the thin films was much different dunring the infrared range. The refractive index and extinction coefficient was adjusted by $Ar:O_2$ ratio in the near-infrared ranges. Variable energy positron annihilation spectroscopy and X-ray photoelectron spectroscopy pointed out that the intrinsic defects resulted in different optical properties, which were fulfilled by regulating the content of oxygen during the deposition process. The localized states theory and the surface dipole mode of the plasmon oscillation of the nanoparticle were applied to explain the low near-infrared transmittance of WO_{3-x} thin films. The samples sputtered at the $Ar:O_2$ ratio of 60:3 showed the best infrared shielding. The optical properties could be tuned by the oxygen partial pressure directly. The lower oxygen content, the more defects, and therefore the better shielding properties. The low infrared transmittance thin films were beneficial for energy conservation with reducing air conditioning usage. The films also could be applied in other shielding fields. The manufacturing technology is convenient and

inexpensive. The switchable thin film can be obtained easily, just tuning the oxygen ratio during sputtering process.

Acknowledgements

This study was financially supported by the high-tech project of MOST (2014AA032802), the national sci-tech support plan the National Natural Science Foundation of China (NSFC, No.: 51272273, 51272271)

Notes and references

1. C. G. Granqvist, *Sol. Energy Mater. Sol. Cells*, 2007, **91**, 1529-1598.
2. A. Kloppel, B. Meyer and J. Trube, *Thin Solid Films*, 2001, **392**, 311-314.
3. E. Ando and M. Miyazaki, *Thin Solid Films*, 2001, **392**, 289-293.
4. G. Zhao, Y. Ren, Y. Gao and J. Shen, in *Eco-Materials Processing and Design Xi*, eds. H. S. Kim, J. F. Yang, T. Sekino, M. Anpo and S. W. Lee, 2010, vol. 658, pp. 81-84.
5. T. Godfroid, R. Gouttebaron, J. P. Dauchot, P. Leclere, R. Lazzaroni and M. Hecq, *Thin Solid Films*, 2003, **437**, 57-62.
6. M. Vergohl, N. Malkomes, T. Matthee, G. Brauer, U. Richter, F. W. Nickol and J. Bruch, *Thin Solid Films*, 2001, **392**, 258-264.
7. A. B. Glot, A. V. Gaponov and A. P. Sandoval-Garcia, *Physica B*, 2010, **405**, 705-711.
8. V. Eyert, *Annalen Der Physik*, 2002, **11**, 650-702.
9. C. G. Granqvist, *Sol. Energy Mater. Sol. Cells*, 2000, **60**, 201-262.
10. S. K. Deb, *Appl Opt*, 1969, **8 Suppl 1**, 192-195.
11. G. A. Niklasson and C. G. Granqvist, *J. Mater. Chem.*, 2007, **17**, 127-156.
12. C. Santato, M. Odziemkowski, M. Ulmann and J. Augustynski, *J. Am. Chem. Soc.*, 2001, **123**, 10639-10649.
13. L. Berggren and G. A. Niklasson, *Solid State Ion.*, 2003, **165**, 51-58.
14. M. B. Johansson, B. Zietz, G. A. Niklasson and L. Osterlund, *J. Appl. Phys.*, 2014, **115**, 7.
15. J. L. Solis, S. Saukko, L. Kish, C. G. Granqvist and V. Lantto, *Thin Solid Films*, 2001, **391**, 255-260.
16. P. J. Shaver, *Appl. Phys. Lett.*, 1967, **11**, 255-&.
17. A. Kubacka, B. Bachiller-Baeza, G. Colon and M. Fernandez-Garcia, *Applied Catalysis B-Environmental*, 2010, **93**, 274-281.
18. J. Yu and L. Qi, *Journal of Hazardous Materials*, 2009, **169**, 221-227.
19. J. S. Hale and J. A. Woollam, *Thin Solid Films*, 1999, **339**, 174-180.
20. E. B. Franke, C. L. Trimble, M. Schubert, J. A. Woollam and J. S. Hale, *Appl. Phys. Lett.*, 2000, **77**, 930-932.
21. C. S. Guo, S. Yin and T. Sato, *Nanoscience and Nanotechnology Letters*, 2011, **3**, 413-416.
22. K. Adachi, Y. Ota, H. Tanaka, M. Okada, N. Oshimura and A. Tofuku, *J. Appl. Phys.*, 2013, **114**, 11.
23. Y. Sato, M. Terauchi and K. Adachi, *J. Appl. Phys.*, 2012, **112**, 7.
24. K. Manthiram and A. P. Alivisatos, *J. Am. Chem. Soc.*, 2012, **134**, 3995-3998.
25. K. Adachi and T. Asahi, *J. Mater. Res.*, 2012, DOI: 10.1557/jmr.2012.25, 1-6.
26. K. Sauvet, A. Rougier and L. Sauques, *Sol. Energy Mater. Sol. Cells*, 2008, **92**, 209-215.
27. C. S. Guo, S. Yin, P. L. Zhang, M. Yan, K. Adachi, T. Chonan and T. Sato, *J. Mater. Chem.*, 2010, **20**, 8227-8229.
28. C. Hu, G. Y. Xu and X. M. Shen, *J. Alloy. Compd.*, 2009, **486**, 371-375.
29. K. Chiba and S. Kaminishi, *Jpn. J. Appl. Phys.*, 2008, **47**, 240-243.
30. K. Chiba, T. Takahashi, T. Kageyama and H. Oda, *Appl. Surf. Sci.*, 2005, **246**, 48-51.
31. F. Z. Tepehan, F. E. Ghodsi, N. Ozer and G. G. Tepehan, *Sol. Energy Mater. Sol. Cells*, 1999, **59**, 265-275.
32. S. K. Gullapalli, R. S. Vemuri and C. V. Ramana, *Appl. Phys. Lett.*, 2010, **96**, 3.

33. B. W. Faughnan and R. S. Crandall, *Appl. Phys. Lett.*, 1977, **31**, 834-836.
34. I. G. Austin and N. F. Mott, *Adv Phys*, 1969, **18**, 41-&.
35. H. D. Zheng, J. Z. Ou, M. S. Strano, R. B. Kaner, A. Mitchell and K. Kalantar-Zadeh, *Adv. Funct. Mater.*, 2011, **21**, 2175-2196.
36. P. Roussel, P. Labbe and D. Groult, *Acta Crystallographica Section B-Structural Science*, 2000, **56**, 377-391.
37. F. Y. Xie, L. Gong, X. Liu, Y. T. Tao, W. H. Zhang, S. H. Chen, H. Meng and J. Chen, *Journal of Electron Spectroscopy and Related Phenomena*, 2012, **185**, 112-118.
38. O. Y. Khyzhun, *J. Alloy. Compd.*, 2000, **305**, 1-6.
39. Z. J. Zhu, M. Y. Yao, X. D. Xue, Y. C. Wu and B. X. Zhou, *13th International Workshop on Slow Positron Beam Techniques and Applications (Slopos13)*, 2014, **505**, 4.
40. I. Prochazka, J. Cizek, O. Melikhova, W. Anwand, G. Brauer, T. E. Konstantinova and I. A. Danilenko, *13th International Workshop on Slow Positron Beam Techniques and Applications (Slopos13)*, 2014, **505**, 4.
41. H. Hagihara, K. Ito, N. Oshima, A. Yabuuchi, H. Suda and H. Yanagishita, *Desalination*, 2014, **344**, 86-89.